BMC Medical Imaging

RESEARCH

Open Access

Unsupervised radiomics-driven endotyping of chronic rhinosinusitis with nasal polyps: a multimodal characterization of CT imaging, clinical phenotypes, and proteomic profiling

Hongfei Zhao[1,2,4†], Qi Wang[3,5,6†], Yan Hao[1,2,8†], Pengyi Yu[1,2,4], Jingjing Li[9], Jianwei Wang[1,2,4], Haicheng Zhang[3,5,6], Yu Zhang[1,2,4], Yujuan Yang[1,2,4], Yakui Mou[1,2,4], Ning Mao[1,3,5,6,7*] and Xicheng Song[1,2,4*]

Abstract

Background The current phenotyping of chronic rhinosinusitis with nasal polyps (CRSwNP) into eosinophilic (eCRSwNP) and non-eosinophilic (non-eCRSwNP) subtypes is increasingly insufficient to address complex clinical challenges, especially as some non-eCRSwNP patients have poor prognoses. Identifying intrinsic endotypes non-invasively is crucial for precision therapy. To identify CRSwNP endotypes via unsupervised clustering of paranasal sinus computed tomography (CT) radiomics features and analyze their clinical and biological significance.

Methods Retrospective study of CRSwNP patients undergoing functional endoscopic sinus surgery (FESS) (Jan 2016-Apr 2021) with preoperative CT. Clustering analysis was performed on patients using 1409 radiomic features. Proteomics analyzed nasal polyps from 41 patients. Clinical characteristics and prognoses were compared.

Results In total, 661 patients were included (median age, 50 years; interquartile range, 40–60 years; 213 [32%] women). Three radiomic clusters were identified. Endotype 3 had the worst prognosis, followed by endotype 1; endotype 2 had the best prognosis (log-rank test, $P = 0.026$ / 0.0026). Endotype 3 exhibited the lowest lymphocyte count (Kruskal-Wallis test, $P = 0.049$), highest CT scores ($P < 0.0001$) and nasal endoscopic scores ($P < 0.0001$). Endotype 3 showed enrichment in inflammatory pathways (complement activation, immune signaling, humoral response). Endotype 2 correlated with lipoprotein processes. Endotype 1 (intermediate prognosis) showed co-enrichment of lipoprotein and inflammatory pathways.

Conclusion Unsupervised CT radiomics clustering identified three prognostically distinct CRSwNP endotypes with differing clinical and biological features. This provides a novel non-invasive method for endotyping and prognostic assessment.

†Hongfei Zhao, Qi Wang and Yan Hao should be considered joint first authors.

*Correspondence:
Ning Mao
maoning@pku.edu.cn
Xicheng Song
drxchsong@163.com

Full list of author information is available at the end of the article

Keywords Radiomics, Consensus clustering, Endotypes, Chronic rhinosinusitis with nasal polyps, Proteomic

Introduction

Chronic rhinosinusitis with nasal polyps (CRSwNP) is a chronic inflammatory disorder of the paranasal sinuses, affecting approximately 1–4% of the global population [1]. The economic burden of CRSwNP is substantial, estimated at $5.7 billion annually in the United States alone [2]. On the basis of the histologic quantification of the numbers of eosinophilic, CRSwNP has generally been categorized into eosinophilic (eCRSwNP) and non-eosinophilic phenotypes (non-eCRSwNP). eCRSwNP patients often require contouring surgery combined with post-op systemic corticosteroids, yet still show higher recurrence rates. In contrast, non-eCRSwNP patients achieve effective control through FESS alone and have low recurrence rate [3–5]. Although classification based on histological features (non-eCRSwNP vs. eCRSwNP) holds certain value in guiding basic treatment, significant heterogeneity remains among patients within the same phenotype. For instance, among patients classified as non-eCRSwNP, most individuals respond well to corticosteroid therapy, while some are prone to recurrence or even develop refractory disease. This heterogeneity may stem from differences in endogenous pathological mechanisms (e.g., Th2 inflammation dominance, IL-5/IL-13 pathway activation variability) [6] or interactions with exogenous comorbidities (e.g., asthma, aspirin-exacerbated respiratory disease), ultimately leading to uncertainties in treatment response and prognostic stratification [7]. However, there is currently no standardized endotyping system for CRSwNP. There is a pressing need to develop novel approaches for endotyping CRSwNP to guide precision management.

While molecular data from tissue biopsies have been explored for CRSwNP typing [8], its invasiveness, spatial heterogeneity, and cost limit clinical adoption. Paranasal sinus CT has multiple advantages such as wide availability, multiplanar imaging for full evaluation, and preoperative classification guidance. Radiomics extracts quantitative imaging features across macroscopic-microbiological scales [9–11], linking tissue phenotypes to prognosis and treatment response [12, 13]. Unsupervised clustering of CT features has been effectively utilized for disease phenotyping. For instance, in patients with sarcoidosis, various features were clustered using unsupervised methods to establish phenotypes associated with inflammatory activity measured by 18FDG - PET/CT [14]. Similarly, in lung cancer and head-and-neck cancer, unsupervised clustering of radiomic features capturing intratumoral heterogeneity has identified subtypes associated with genomic mutations and survival outcomes [15]. These studies underscore the versatility of radiomics in uncovering disease heterogeneity beyond conventional diagnostic criteria. However, there is currently no research on unsupervised clustering of radiomics for CRSwNP. With the increasing use of protein sequencing, integrate radiomics and proteomics analysis may guide disease typing and treatment [16]. To date, no studies have integrated proteomics to elucidate the biological mechanisms underlying radiomics-based endotyping in patients with CRSwNP.

This study redefined endotyping in CRSwNP through unsupervised clustering of CT radiomic features, identifying three distinct subtypes with divergent prognostic trajectories. Furthermore, we integrated proteomic findings to elucidate the biological underpinnings of the endotypes. These new insights not only allow us to decipher CRSwNP molecular heterogeneity through radiological features, but also provide an innovative non-invasive solution for CRSwNP endotyping.

Materials and methods

Study design and research strategy

This study employed a retrospective, multimodal cohort design to discover and characterize novel endotypes in CRSwNP. The overall strategy followed a sequential workflow integrating radiomics, clinical phenotyping, and proteomics. First, we aimed to identify data-driven endotypes by applying unsupervised consensus clustering to high-dimensional radiomic features extracted from preoperative paranasal sinus CT scans, independent of existing phenotypic classifications. Second, to validate the clinical relevance of the identified endotypes, we compared them against comprehensive clinical characteristics and assessed their association with long-term postoperative disease control. Finally, exploratory proteomic profiling of nasal polyp tissues from a subset of patients was performed to investigate differentially expressed proteins and pathways across endotypes, with the goal of linking imaging-based subtypes to potential molecular mechanisms. We hypothesized that CT radiomic features capture intrinsic tissue heterogeneity corresponding to distinct disease endotypes with divergent clinical outcomes and biological signatures. This integrative approach was designed to combine non-invasive radiomics for subtype discovery with proteomics for biological insight, thereby exploring potential connections between imaging patterns and underlying molecular mechanisms.

Study sample

The study protocol was approved by the Human Ethics Committee of Yantai Yuhuangding Hospital, Qingdao

University (approval number: 2025-098) and conducted according to the principles of the Declaration of Helsinki. The requirement for written informed consent was partially waived for the retrospective study. Written informed consent was obtained from each patient before nasal polyp tissue sample collection.This analysis was performed on patients who underwent FESS and were pathologically diagnosed with CRSwNP from January 2016 to April 2021. All the patients satisfied the following inclusion criteria: (1) meeting the criteria for CRSwNP as defined by the European Position Paper on Rhinosinusitis and Nasal Polyps 2020 guidelines [17]; (2) no history of nasal surgery, normal liver and kidney function; (3) no oral corticosteroids or macrolide antibiotics taken within one month prior to treatment. The exclusion criteria were: (1) patients who did not receive a sinuses CT scan within 2 weeks before surgery; (2) blurred CT images; (3) fungal rhinosinusitis; (4) antrochoanal polyp; (5) nasal and sinus tumors; (6) cystic fibrosis; (7) history of head and neck radiotherapy; (8) patients lacking complete clinical data. This study initially included 908 patients with CRSwNP, among them, 866 patients had undergone a sinus CT scan within 2 weeks before surgery. The patient inclusion workflow is shown in Supplementary Figure S1.

Patient data collection and prognosis assessment

The clinical data of the patients, including clinical features (age, gender), clinically relevant diseases (asthma, allergic rhinitis), previous sinus surgery history, CT score, and nasal polyp score, and tissue/peripheral inflammatory cell counts, were collected from the hospital information system. The nasal polyps were also scored according to the Lund-Kennedy and Lund-Mackay score staging system prior to surgery [18, 19]. Patients were followed up postoperatively every 3 to 6 months for at least 24 months (46 [33–51] months). Patient prognosis was assessed based on clinical symptoms (including nasal blockage, rhinorrhoea/postnasal drip, facial pain/pressure, olfactory dysfunction, sleep disturbance, and fatigue), nasal endoscopic findings of diseased mucosa, and rescue treatment within the preceding 6 months. Disease control status was categorized using a visual analogue scale (VAS, 0–10) as: controlled (no symptoms present), partly controlled (1–2 symptoms present), or uncontrolled (≥ 3 symptoms present). The detailed criteria can be referred to EPOS 2020 [17]. When analyzing differences in disease control levels, the three-category classification (controlled, partly controlled, uncontrolled) was dichotomized into either: "controlled" versus "partly controlled + uncontrolled" or "controlled + partly controlled" versus "uncontrolled".

CT image acquisition

The imaging protocol employed two multidetector CT systems: a GE LightSpeed 64-slice scanner (General Electric Healthcare, USA) and a Philips iCT 256-slice scanner (Philips Healthcare, Netherlands). DICOM-formatted datasets were extracted from the institutional PACS, with standardized acquisition parameters maintained at 120 kV tube voltage, 300 mA current, and 512 × 512 pixel matrix. Axial images were reconstructed using 5 mm slice thickness with 1.25 mm overlapping intervals. Sinus-specific window settings (width 350 HU/level 40 HU) were uniformly applied for optimal soft tissue-bone differentiation. Figure 1 shows our workflow.

CT segmentation

We selected axial images between the onset of the bilateral inferior turbinate and frontal lobe. ITK-SNAP software (version 3.8.0) was utilized by two radiologists, Dr. A with 6 years and Dr. B with 10 years of experience in paranasal sinus imaging, to manually delineate the region of interest (ROI) of the entire sinonasal cavity. This process was overseen by Dr. C, a radiologist with 25 years of expertise in paranasal sinus imaging. Three radiologists were aware of the diagnosis of CRSwNP but were blinded to the clinical and histopathologic data.

Radiomics feature extraction

Radiomic features were extracted using PyRadiomics 3.0.1 (https://pyradiomics.readthedocs.io/en/latest/index.html). All images were isotropically resampled to a voxel spacing of $1 \times 1 \times 1$ mm^3 using cubic B-spline interpolation. Intensity normalization was subsequently applied to reduce inter-scanner variability and standardize feature calculation. The extracted features encompassed divided into shape features, first-order statistics, wavelet features, neighborhood gray-tone difference matrix (NGTDM), gray-level size zone matrix (GLSZM), grey level run length matrix (GLRLM) features, gray-level dependence matrix (GLDM), and gray-level co-occurrence matrix (GLCM). To reduce inter-scanner and inter-protocol variability, ComBat harmonization was applied to the extracted radiomic feature matrix using the Python-based neuroCombat package for batch-effect correction.

Inter- and intra-class correlation coefficients (ICCs) were calculated to assess the reproducibility of the radiomics features. One month later, two segmenters randomly selected 30 patients and repeated the delineation process. Intra-observer and inter-observer ICCs were then calculated. Features with ICC > 0.75 were considered to have good reproducibility. Features that could not be consistently computed across all patients were excluded from subsequent analysis. All remaining reproducible features were included in the consensus

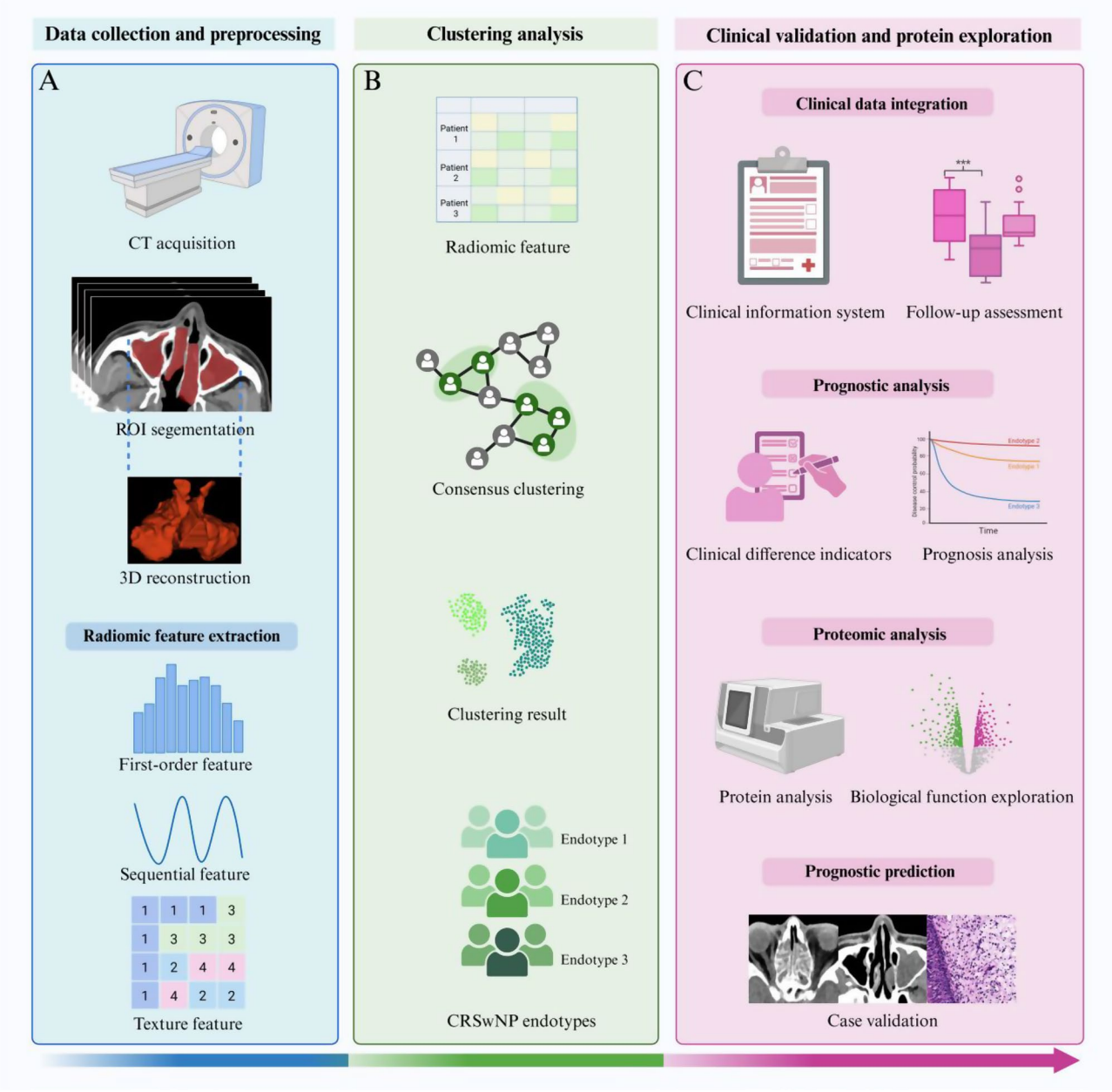

Fig. 1 Workflow of this study. (**A**) Radiomics feature extraction from CT scans of CRSwNP patients; (**B**) The radiomics features of CRSwNP patients were clustered into three categories using consensus clustering; (**C**) Analysis of clinical features, differences in prognosis and proteomics characteristics of CRSwNP patients. With the exception of the CT and pathology images presented in Fig. 1, all illustrations were produced with BioRender (https://biorender.com). CT, computed tomography; CRSwNP, chronic rhinosinusitis with nasal polyps

clustering analysis to comprehensively capture the full spectrum of imaging heterogeneity.

Sensitivity analysis of feature preprocessing

To evaluate the robustness of the identified endotypes to feature selection and dimensionality reduction, we conducted a sensitivity analysis using a sequential preprocessing pipeline. First, features with variance below 0.08*(1-0.08) were removed. Next, features with an absolute Spearman correlation coefficient > 0.9 were removed. Finally, principal component analysis (PCA) was applied to the resulting filtered set, and components explaining > 95% of cumulative variance were retained. All clustering parameters remained identical to the primary analysis.

Consensus clustering

We performed consensus clustering using the ConsensusClusterPlus package in R. The analysis was configured with maxK = 6, reps = 50, pItem = 0.8, pFeature = 1, and a

fixed random seed. For each candidate k (2–6), a consensus matrix was generated.

We used the Partitioning Around Medoids (PAM) algorithm within the ConsensusClusterPlus framework in this study [20]. PAM is a clustering method based on representative objects (medoids), which is conceptually similar to K-means clustering. However, unlike K-means, PAM selects actual data points within the dataset as cluster representatives (i.e., medoids) rather than computing mean values. PAM optimizes the clustering results by iteratively adjusting the medoids and reassigning data points to their nearest medoid [21]. The detail of the PAM algorithm was shown in the Supplementary materials.

The optimal cluster number k = 3 was determined by evaluating the consensus matrix structure (Supplementary Figure S2A), the relative change in area under the cumulative distribution function (CDF) curve (Supplementary Figure S2B), and the tracking plot (Supplementary Figure S2C). Cluster stability was quantified using the calcICL function, which yielded high cluster-consensus (Supplementary Figure S2D) and item-consensus (Supplementary Figure S2E) values for the three-cluster solution. Sensitivity to sampling variability was assessed through the built-in resampling (50 iterations, 80% subsampling), confirming the robustness of the three endotypes.

External validation cohort

To assess generalizability, an independent cohort of 270 consecutive CRSwNP patients who underwent FESS at Peking Union Medical College Hospital between January 2016 and January 2023 was assembled using the same inclusion and exclusion criteria as the original study. CT images were acquired using a 64-slice spiral CT scanner (Sensation 64; SIEMENS, Germany) or a 256-slice spiral CT scanner (Sensation 256; Philips, Netherlands), and radiomic features were extracted following an identical pipeline. The same analytical procedure was employed for unsupervised clustering analysis.

Sample selection

Protein sequencing analysis was performed in 41 patients to explore the differences in biological characteristics among different endotypes. These patients were consecutively selected based on the availability of sufficient, high-quality fresh-frozen tissue obtained during FESS, ensuring technical feasibility while minimizing selection bias. The endotype distribution within this proteomics subset was highly consistent with that of the overall cohort (Supplementary Figure S3), with no statistically significant difference confirmed by a Chi-square goodness-of-fit test ($\chi^2(2) = 1.27$, $P = 0.53$). All enrolled patients had comprehensive clinical data, enabling correlative analysis between proteomic findings and clinical features or prognostic outcomes.

Protein extraction and LC-MS/MS analysis

Following surgical resection, tissue specimens were snap-frozen and stored at − 80 °C. Proteins were extracted by homogenizing frozen tissues in RIPA buffer containing protease inhibitors. After centrifugation, lysates were reduced, alkylated, and digested with trypsin to generate peptides. Peptide separation was performed on a nano-flow C18 column (EASY-Spray™, 75 μm × 50 cm) using a gradient elution, and analysis was carried out on a Q Exactive HFX mass spectrometer coupled with an Easy nLC 1200 system in data-independent acquisition (DIA) mode. System stability was monitored using pooled quality-control samples; criteria included a quantification coefficient of variation < 20%, clustering in principal component analysis, inter-sample correlation > 0.9, chromatographic peak density ≥ 5 points/peak, column peak capacity, and stable retention times of iRT internal standards. Raw data were processed in Spectronaut™ (v14.4.200727.47784) against the UniProt human proteome database, requiring ≥ 2 unique peptides and a false discovery rate ≤ 1% at both peptide and protein levels. Protein intensities were median-normalized, and differential expression between the three clusters was determined using DESeq2 with thresholds of $|\log_2$ fold change$| \geq 2$ and FDR-adjusted $P < 0.05$.

Functional enrichment analysis

Gene Ontology (GO) database ("clusterProfiler" package in R) was employed to compare protein enriched pathways between the three groups of patients. Pathway enrichment analysis was also conducted by Kyoto Encyclopaedia of Genes and Genomes (KEGG) database Proteomic characterization analysis was performed using pairwise comparisons, where one cluster was selected and compared with combinations of the other two clusters.

Statistical analysis

All statistical analyses were performed by SPSS 20.0 (IBM, Armonk, USA), a R software (version 3.6.2, www.r-project.org) and Python (version3.6.6). The ANOVA test or Kruskal-Wallis method was used to compare continuous variables, and categorical variables were performed using the chi-square test or Fisher's exact test. The significance of correlations was assessed using the Pearson correlation test or the Spearman correlation test. The prognosis of the patients was analyzed by using the Kaplan-Meier curve, and the prognostic differences between endotypes were assessed using log-rank tests. Variables with $P < 0.05$ in univariate Cox proportional hazards regression analyses and without multicollinearity

Table 1 Demographic, cytology, clinical examination, and follow-up information of all patients

Characteristic	All
	(*n* = 661)
Sex	
Gender (Male)	448 (67.8)
Gender (Female)	213 (32.2)
Age	50 (40–60)
Smoking history	
yes, n (%)	219 (33.1)
no, n (%)	442 (66.9)
Current alcohol use	
yes, n (%)	183 (27.7)
no, n (%)	478 (72.3)
FESS surgery history	
yes, n (%)	17 (2.6)
no, n (%)	644 (97.4)
Symptoms duration (months)	7 (2–24)
Comorbid asthma	
yes, n (%)	107 (16.2)
no, n (%)	554 (83.8)
Comorbid allergic rhinitis	
yes, n (%)	91 (13.8)
no, n (%)	570 (86.2)
Inflammatory cell count (histopathology, n/HFP)	149.17 (107.8-211.1)
Eosinophils (histopathology, n/HFP)	25.17 (8.5-41.27)
Eosinophils (histopathology, %)	18.19 (6.38–30.55)
Neutrophils (histopathology, n/HFP)	8.67 (1.2-16.92)
Neutrophils (histopathology, %)	6.34 (1.18–10.91)
Plasmocyte (histopathology, n/HFP)	15 (9-37.8)
Lymphocyte (histopathology, n/HFP)	79.2 (38.1-106.83)
Eosinophils (peripheral blood, *n*×10^9/L)	0.21 (0.1–0.35)
Basophils (peripheral blood, *n*×10^9/L)	0.04 (0.03–0.06)
Neutrophils (peripheral blood, *n*×10^9/L)	3.35 (2.61–4.25)
Lymphocyte (peripheral blood, *n*×10^9/L)	1.96 (1.62–2.44)
Ethmoid-to-maxillary sinus ratio	1.67 (1.33–2.33)
LM score	11 (6–16)
Nasal polyp score	3 (2–4)
Postoperative follow-up interval (months)	46 (33–51)

Note: HFP, high power field. LM score, Lund-Mackay CT Score. Continuous variables were presented as median (interquartile range) or mean ± standard deviation, and categorical variables as absolute numbers with relative frequencies (percentages)

(VIF < 4) were included in the multivariate analyses, and hazard ratios (HR) and 95% confidence intervals (CI) were calculated to assess prognostic factors associated with disease control status. All hypothesis tests were two sided, and $P < 0.05$ was considered statistically significant.

Results

Clinical characteristics of the study population

Of 908 patients identified with CRSwNP, 661 met the inclusion criteria (448 men and 213 women). Median age of the patients was 50 years (interquartile range [IQR], 40–60 years). Most patients were not smokers ($n = 442$ [67%]) or drinker ($n = 478$ [72%]). Most of the patients did not have combined asthma ($n = 554$ [84%]) or allergic rhinitis ($n = 570$ [86%]). At admission, the median CT score was 11 (IQR, 6–16), and the median endoscopic score was 3 (IQR, 2–4). Detailed information on demographic and clinical characteristics is presented in Table 1.

Reproducibility and radiomics feature set

A total of 1688 radiomic features were initially extracted. After excluding features that could not be successfully computed across all patients, 1409 valid radiomics features were retained. Intra-observer and inter-observer reproducibility assessments in the 30 randomly selected patients demonstrated excellent agreement, with inter-observer ICCs ranging from 0.82 to 0.92 and intra-observer ICCs ranging from 0.86 to 0.94, indicating that the extraction of radiomics features exhibited good reproducibility.

Consensus clustering associations

Clustering analysis of 1409 radiomic features showed that when K = 3, the relative change in the area under the cumulative distribution function curve decreased sharply (Fig S2), and CRSwNP patients were accordingly divided into three robust clusters (Fig. 2A). Demographic, cytology, clinical examination, and follow-up information of the three endotypes were summarized in Table 2. Some differences in clinical characteristics were observed across endotypes. Patients in endotype 3 exhibited the lowest lymphocyte count in nasal polyp tissues (Kruskal-Wallis test, 75.75 [38-101.25], $P = 0.049$). Furthermore, their CT scores (Kruskal-Wallis test, 13 [7–20], $P < 0.0001$) and nasal endoscopy scores (Kruskal-Wallis test, 4 [3–5], $P < 0.0001$) were higher than the other endotypes (Fig. 2B). There were no statistically significant differences in eosinophil counts between the three clusters either in tissue ($P = 0.719$) or in peripheral blood ($P = 0.426$), suggesting that CRSwNP typing based on radiomics features was distinctive and independent of eosinophil count, whereas previous studies had relied on eosinophil counts to distinguish CRSwNP endotypes.

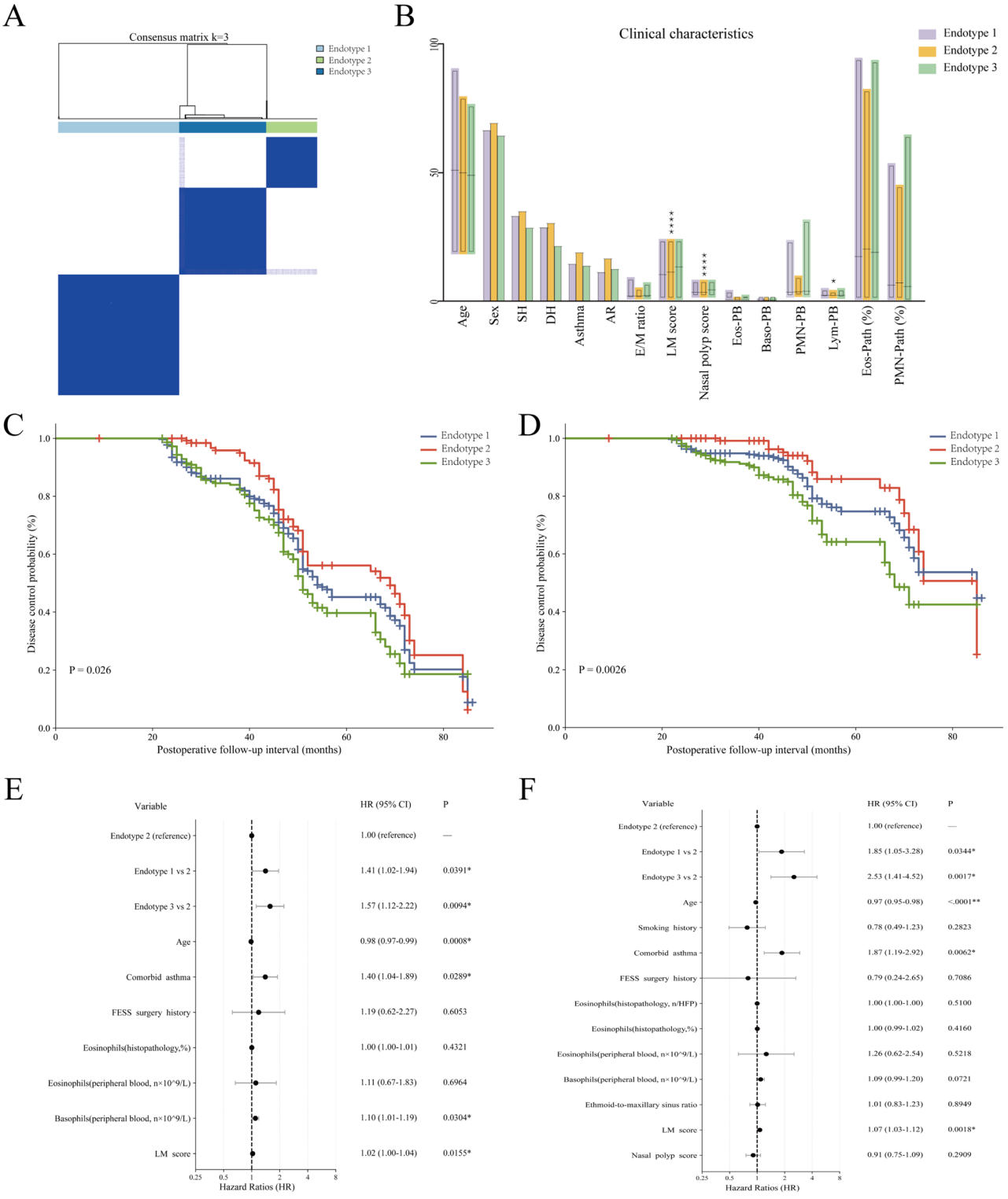

Fig. 2 (See legend on next page.)

According to EPOS 2020 criteria, when classified by "controlled" versus "partly controlled+ uncontrolled", Kaplan-Meier analysis revealed superior prognosis in endotype 2, intermediate in endotype 1, and poorest in endotype 3 ($P = 0.026$) (Fig. 2C). Consistent results were observed when dichotomized as "controlled+ partly controlled" versus "uncontrolled" ($P = 0.0026$) (Fig. 2D). Collectively, the analysis demonstrated that CT-based

(See figure on previous page.)

Fig. 2 CRSwNP endotypes based on radiomic consensus clustering and their clinical differences. (**A**) Conditional density function demonstrating consensus clustering of radiomic features at a k value of 3. (**B**) Clinical characteristics of three endotypes. Endotype 3 exhibited the lowest lymphocyte infiltration in nasal polyps and the highest Lund-Kennedy CT and Lund-Mackay endoscopic scores, (*$P < 0.05$, ****$P < 0.0001$). Box plots, continuous variables; bars, categorical variables. (**C**) When categorized as "controlled" versus "partly controlled + uncontrolled", Kaplan-Meier analysis demonstrated that endotype 2 had the best prognosis, endotype 1 showed intermediate outcomes, and endotype 3 exhibited the poorest prognosis, ($P = 0.026$). (**D**) When categorized as "controlled+ partly controlled" versus "uncontrolled", Kaplan-Meier analysis revealed superior prognosis in endotype 2, intermediate in endotype 1, and poorest in endotype 3, ($P = 0.0026$). (**E**) Multivariable Cox regression forest plot for "controlled" vs. "partly controlled + uncontrolled" disease states. (**F**) Multivariable Cox regression forest plot for "controlled + partly controlled" vs. "uncontrolled" disease states. Endotype was consistently identified as a strong independent predictor in both models. SH, smoking history. Asthma, combined with asthma. DH, drinking history. AR, combined with allergic rhinitis. E/M ratio, ethmoid-to-maxillary sinus ratio. LM score, Lund-Mackay CT score. Eos-PB, eosinophils, (peripheral blood, *n*×10^9/L). Baso-PB, basophils, (peripheral blood, *n*×10^9/L). PMN-PB, neutrophils, (peripheral blood, *n*×10^9/L). Lym-PB, lymphocyte, (peripheral blood, *n*×10^9/L). Eos-Path, (%), eosinophils, (histopathology, %). PMN-Path, (%), neutrophils, (histopathology, %)

radiomic profiling captured clinical and prognostic differences in CRSwNP that were complementary to the information provided by routine clinical, functional, and imaging tests. To further identify independent prognostic factors, we performed Cox proportional hazards regression analyses. In the multivariable model, we incorporated significant variables associated with disease control identified from the univariate analysis (Supplementary Figure S4) along with key clinical covariates such as FESS surgery history. The results demonstrated that endotype classification remained the strongest independent predictor of disease control status. In the model comparing "Controlled" versus "Partly Controlled + Uncontrolled" states (Fig. 2E), both Endotype 1 (HR = 1.41, 95% CI: 1.02–1.94) and Endotype 3 (HR = 1.57, 95% CI: 1.12–2.22) were associated with a significantly increased risk of worse outcomes compared to Endotype 2. The prognostic risk conferred by endotype was even more pronounced in the model for "Controlled + Partly Controlled" versus "Uncontrolled" disease (Fig. 2F), with Endotype 1 and Endotype 3 showing substantially higher hazard ratios of 1.85 and 2.53, respectively. Furthermore, comorbid asthma was identified as a significant independent risk factor in both models, a finding consistent with the established immunological consensus that asthma and CRSwNP both belong to the "type 2 inflammation" category.

External validation of radiomic endotypes

The validation cohort included 270 patients. Kaplan-Meier analysis demonstrated significant differences in disease control among the three endotypes, as shown in Supplementary Figures S5A and S5B. Consistent with the discovery cohort, Endotype 2 exhibited the most favorable prognosis, Endotype 3 the poorest, and Endotype 1 an intermediate outcome (log-rank $P = 0.0001$ and $P = 0.0056$, respectively). These findings confirm the robustness and reproducibility of the proposed radiomics-based endotyping.

Impact of feature selection on radiomics subtyping performance

To evaluate the influence of feature stability on subtyping, we performed supplementary analyses. First, low-variance features were removed, reducing the feature set from 1409 to 515. Then, highly correlated features were further eliminated, resulting in 140 non-redundant features. Consensus clustering based on this filtered feature set achieved optimal separation at K = 3 (Supplementary Figure S6A, B), but the resulting endotypes showed attenuated prognostic stratification: no statistically significant survival difference was observed between the "Controlled + Partially Controlled" and "Uncontrolled" groups ($P = 0.0773$, Supplementary Figure S6C), and the prognostic pattern between "Controlled" and "Partially Controlled + Uncontrolled" became inconsistent (Supplementary Figure S6D). Based on the 41 principal components derived from PCA of the filtered features (Supplementary Figure S6E), consensus clustering (K = 3, Supplementary Figure S6F, G) restored prognostic distinction between "Controlled" and "Partially Controlled + Uncontrolled" groups (Supplementary Figure S6H), but still failed to stratify "Controlled + Partially Controlled" from "Uncontrolled" patients ($P = 0.1332$, Supplementary Figure S6I), likely due to the loss of higher-order information. In contrast, the clustering model based on the original 1409 high-dimensional features demonstrated statistically significant and consistent stratification across both clinical endpoints (Fig. 2C, D). Therefore, the three endotypes defined using all 1409 features were adopted for subsequent analysis.

Proteomic signatures of different endotypes of CRSwNP

After excluding variables with a fold change < 2 and $P \geq 0.05$, a total of 299 proteins were retained for proteomic functional analysis. As shown in Supplementary Figure S7, the proteomics profiles differ significantly across the endotypes. A total of 147 upregulated differentially expressed proteins (DEPs) and 256 downregulated DEPs were found in endotype 1. Immune- and metabolism-related genes, including FAM3D, BPIB3, CHPT1 and FAH2B, were identified (Fig. 3A). GO

Table 2 Demographic, cytology, clinical examination, and follow-up information of three endotypes

Characteristic	Endotype 1	Endotype 2	Endotype 3	*P*
	(*n* = 309)	(*n* = 130)	(*n* = 222)	
Sex				
Gender (Male)	210 (67.96)	92 (70.77)	146 (65.77)	0.622
Gender (Female)	99 (32.04)	38 (29.23)	76 (34.23)	
Age	50.93 ± 12.58	50 (41–59)	49 (37–60)	0.086
Smoking history				
yes, n (%)	106 (34.3)	47 (36.15)	66 (29.73)	0.389
no, n (%)	203 (65.7)	83 (63.8)	156 (70.3)	
Current alcohol use				
yes, n (%)	92 (29.77)	41 (31.54)	50 (22.52)	0.101
no, n (%)	217 (70.2)	89 (68.5)	172 (77.5)	
FESS surgery history				
yes, n (%)	8 (2.59)	1 (0.77)	8 (3.60)	0.269
no, n (%)	301 (97.4)	129 (99.2)	214 (96.4)	
Symptoms duration (months)	6 (2–24)	6 (2–24)	12 (2–36)	0.24
Comorbid asthma				
yes, n (%)	48 (15.53)	26 (20.00)	33 (14.86)	0.411
no, n (%)	261 (84.5)	104 (80.0)	189 (85.1)	
Comorbid allergic rhinitis				
yes, n (%)	38 (12.3)	23 (17.69)	30 (13.51)	0.455
no, n (%)	271 (87.7)	107 (82.3)	192 (86.5)	
Inflammatory cell count (histopathology, n/HFP)	153.33 (114.17–230.1)	144.5 (98.6-207.25)	147.75 (107.4–198)	0.317
Eosinophils (histopathology, n/HFP)	24 (8.5-40.27)	25.5 (8.9–50.5)	25.83 (8.15–41.05)	0.719
Eosinophils (histopathology, %)	17.24 (5.85–27.27)	20.02 (7.65–37.23)	18.79 (7.24–30.05)	0.298
Neutrophils (histopathology, n/HFP)	9 (1.5-16.83)	9 (1.85-20)	8 (1-15.73)	0.395
Neutrophils (histopathology, %)	5.98 (1.17–11.01)	6.77 (1.70-12.11)	6.11 (0.67–10.36)	0.482
Plasmocyte (histopathology, n/HFP)	15.33 (9.42–39.9)	13.42 (8.96–37.2)	14.35 (8.48–34.75)	0.724
Lymphocyte (histopathology, n/HFP)	85.67 (42-117.75)	77.9 (32-101.04)	75.75 (38-101.25)	0.049
Eosinophils (peripheral blood, *n*×10^9/L)	0.21 (0.1–0.34)	0.23 (0.09–0.4)	0.19 (0.08–0.34)	0.426
Basophils (peripheral blood, *n*×10^9/L)	0.04 (0.03–0.06)	0.04 (0.03–0.05)	0.04 (0.02–0.06)	0.496
Neutrophils (peripheral blood, *n*×10^9/L)	3.23 (2.52–4.11)	3.295 (2.56–4.03)	3.59 (2.70–4.6)	0.014
Lymphocyte (peripheral blood, *n*×10^9/L)	1.98 (1.63–2.43)	1.97 (1.62–2.50)	1.93 (1.62–2.33)	0.542
Ethmoid-to-maxillary sinus ratio	1.67 (1.33–2.33)	1.67 (1.33–2.33)	1.75 (1.33–2.37)	0.858
LM score	10 (6–14)	11 (6.75-16)	13 (7–20)	< 0.0001
Nasal polyp score	3 (2–4)	3 (2–4)	4 (3–5)	< 0.0001
Postoperative follow-up interval (months)	46 (32–53)	47 (42-55.5)	45 (30–50)	< 0.0001

Note: HFP, high power field. LM score, Lund-Mackay CT Score. Continuous variables were presented as median (interquartile range) or mean ± standard deviation, and categorical variables as absolute numbers with relative frequencies (percentages). P-values reflected univariate comparisons between groups using Mann-Whitney U tests for continuous variables and Fisher's exact tests for categorical variables

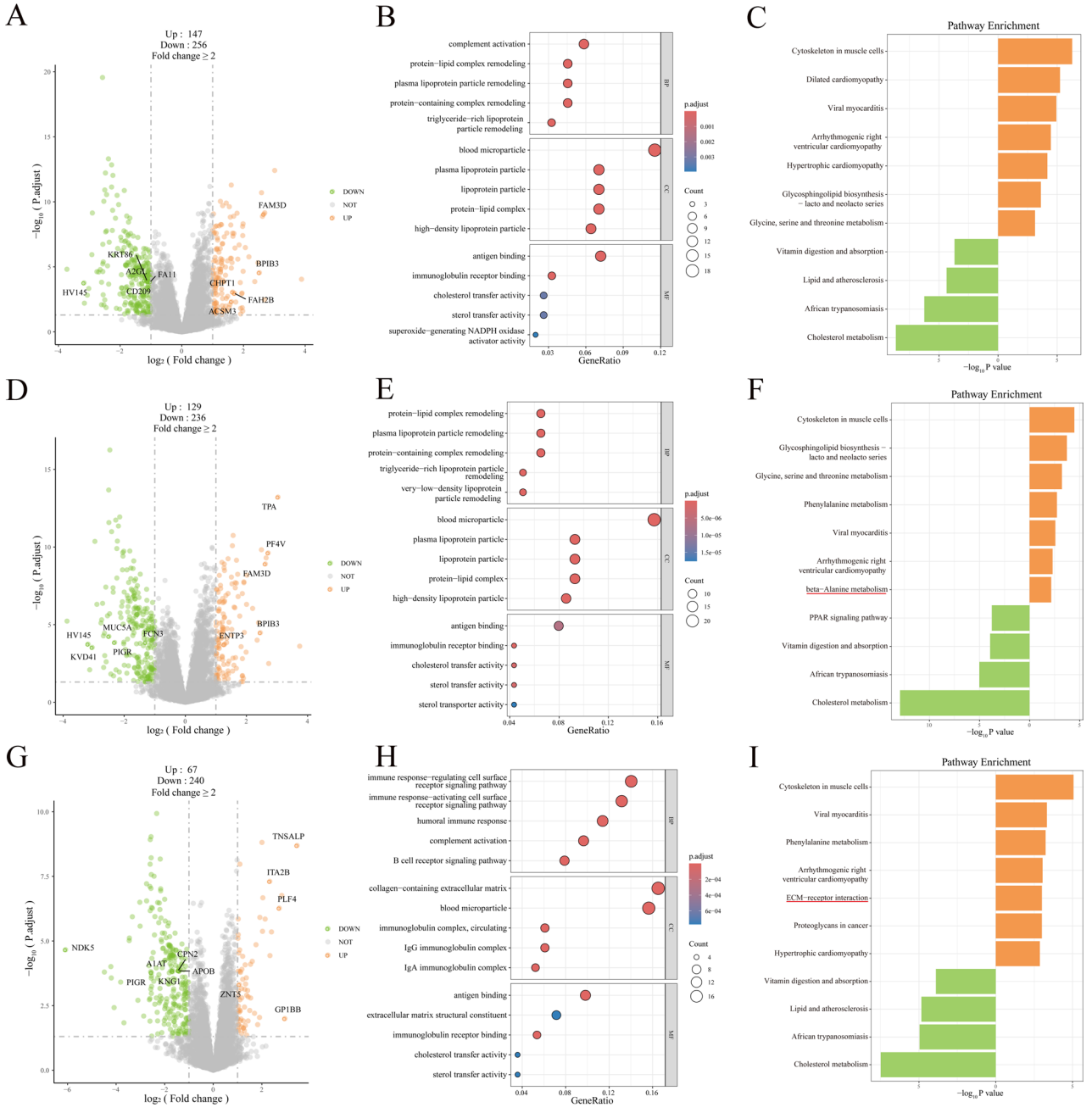

Fig. 3 Biological basis of endotypes. (**A**, **D**, **G**) Volcano plots showed the differential expressed genes in endotypes. Red dots represented proteins up-regulated in the endotypes, whereas blue dots represented proteins down-regulated in the endotypes. The x-axis denoted the fold change, (log2 scale), whereas the y-axis indicated statistical significance, (− log10 format)., (**B**, **E**, **H**) Kyoto Encyclopedia of Genes and Genomes pathway analysis of endotypes proteins was performed., (**C**, **F**, **I**) Gene ontology, (GO) pathway analysis of endotypes proteins was conducted. Red represented up-regulated pathways and blue represented down-regulated pathways

analysis revealed significant upregulation of inflammation-associated biological processes in endotype 1, such as complement activation. Additionally, protein metabolism-related processes including protein-lipid complex remodeling were upregulated. Enriched cellular components were predominantly associated with lipoprotein particles (Fig. 3B). The KEGG analysis revealed an enrichment of metabolism-related pathways (Fig. 3C).

Compared to the other endotypes, endotype 2 demonstrated upregulation of protective genes linked to CRSwNP progression, such as TPA, PF4V, FAM3D, BPIB3, and ENTP3, alongside downregulation of inflammation-related genes (PIGR, FCN3, and HV145)

(Fig. 3D). Upregulated pathways in this endotype were primarily associated with lipoprotein metabolism, with enriched cellular components also dominated by lipoproteins (Fig. 3E). KEGG pathway analysis highlighted lipid and amino acid metabolism, with beta-alanine metabolism uniquely observed in endotype 2 (Fig. 3F).

Endotype 3 showed upregulation of coagulation cascade activation- and angiogenesis-related DEPs and downregulation of metabolism- and tissue repair-associated proteins (Fig. 3G). GO analysis indicated broad activation of innate and adaptive immune responses, including complement activation, B cell receptor signaling pathway, and humoral immune response (Fig. 3H). KEGG analysis further revealed upregulation of the ECM-receptor interaction pathway, which may drive nasal mucosal fibrosis (Fig. 3I).

Prognostic superiority of radiomic clustering: case validation

To validate the prognostic utility of CT radiomic clustering, three representative cases were analyzed. A 62-year-old male with extensive sinonasal inflammation (Lund-Mackay score: 21) (Fig. 4A, B) and eosinophilic polyps (eosinophil density: 31%) (Fig. 4C) was traditionally classified as high-risk due to eosinophil predominance and sinus opacification but assigned to intermediate-prognosis endotype 1 by radiomics. During the 30 months postoperative follow-up, the patient's disease status was classified as "partly controlled", demonstrating superior accuracy of radiomic endotyping. Conversely, a 54-year-old male with similar CT inflammation (Lund-Mackay score: 19) (Fig. 4D, E) and eosinophilic polyps (eosinophil density: 18%) (Fig. 4F) was radiomically stratified into favorable endotype 2, achieving sustained remission ("controlled") after 66 months. This discordance suggests that radiomic features capture compensatory healing patterns overlooked by inflammatory burden metrics. In contrast, a 40-year-old male with non-eCRSwNP (eosinophil density: 0.3%; Lund-Mackay score: 2) (Fig. 4G, H, I) deemed low-risk by conventional criteria was categorized as high-risk endotype 3 by radiomics, experiencing recurrence within 47 months post-FESS. These discrepancies highlight radiomics' ability to detect subclinical structural anomalies that evade phenotypic assessment.

Discussion

This is the first study to classify the endotypes of CRSwNP using an unsupervised clustering analysis of paranasal sinus CT radiomics features, without bias from phenotype data. By employing a consensus clustering algorithm, we identified three distinct CRSwNP endotypic subgroups with significant prognostic divergence. Our approach successfully reclassified cases discordant with conventional prognostic indicators—patients historically deemed high-risk based on histopathological or imaging but exhibiting good postoperative prognosis in actual clinical, which was consistent with the prognostic results represented by the endotypes determined through radiomics clustering. Proteomic profiling further validated the biological uniqueness of these endotypes, revealing endotype-specific molecular pathways correlated with differential clinical outcomes.

Histopathological subtyping offers advantages in revealing microscopic mechanisms [22–25], and prior studies have classified CRS patients based on immune markers in nasal mucosal tissues [22]. Xiangdong Wang et al. identified endotypes in CRS patients using inflammatory and remodeling factors derived from nasal mucosal tissues [26]. However, these approaches are constrained by their invasiveness, high costs, time-intensive workflows, and sampling biases. As an essential preoperative examination for CRS patients, multi-detector sinus CT scans enable prospective guidance for disease subtyping. In contrast, CT-based radiomics provides a non-invasive, rapid, and comprehensive alternative, making it a preferable tool for clinical classification. To our knowledge, no studies to date have explored radiomics for endotyping in CRSwNP. Our work addresses the limitations of traditional research approaches by utilizing CT radiomic features to explore endotypes in CRSwNP.

Unsupervised clustering identifies latent relationships and intrinsic structures within data, operates without predefined labels, and efficiently handles high-dimensional datasets [27]. Earlier studies focused narrowly on eCRSwNP [28], exemplified by K-Z Zhu et al., who developed a CT-based radiomic model for identifying eCRSwNP. Similarly, Hong-Li Hua et al. [29]distinguished eosinophilic and non-eosinophilic CRSwNP using preoperative CT. None of their studies addressed broader endotypic diversity. In contrast, our study used unsupervised radiomics clustering to identify three endotypes with different prognosis and molecular features by capturing multidimensional anatomical heterogeneity.

While numerous studies have leveraged radiomic features for CRSwNP stratification, few have bridged the imaging-to-biology gap. Our study integrated proteomics data to reveal endotype-specific proteins and pathway dysregulations, verifying the biological plausibility of radiomics endotypes. Endotype 2 uniquely displayed elevated tissue-type plasminogen activator (t-PA) levels. Unlike normal mucosa, nasal polyps exhibit t-PA deficiency, leading to fibrin accumulation due to impaired plasmin-mediated fibrinolysis [30–32]. Restored t-PA expression in endotype 2 may enhance fibrin degradation, contributing to its superior postoperative outcomes. Notably, this endotype was strongly linked to lipoprotein-related processes. Multiple studies suggested that

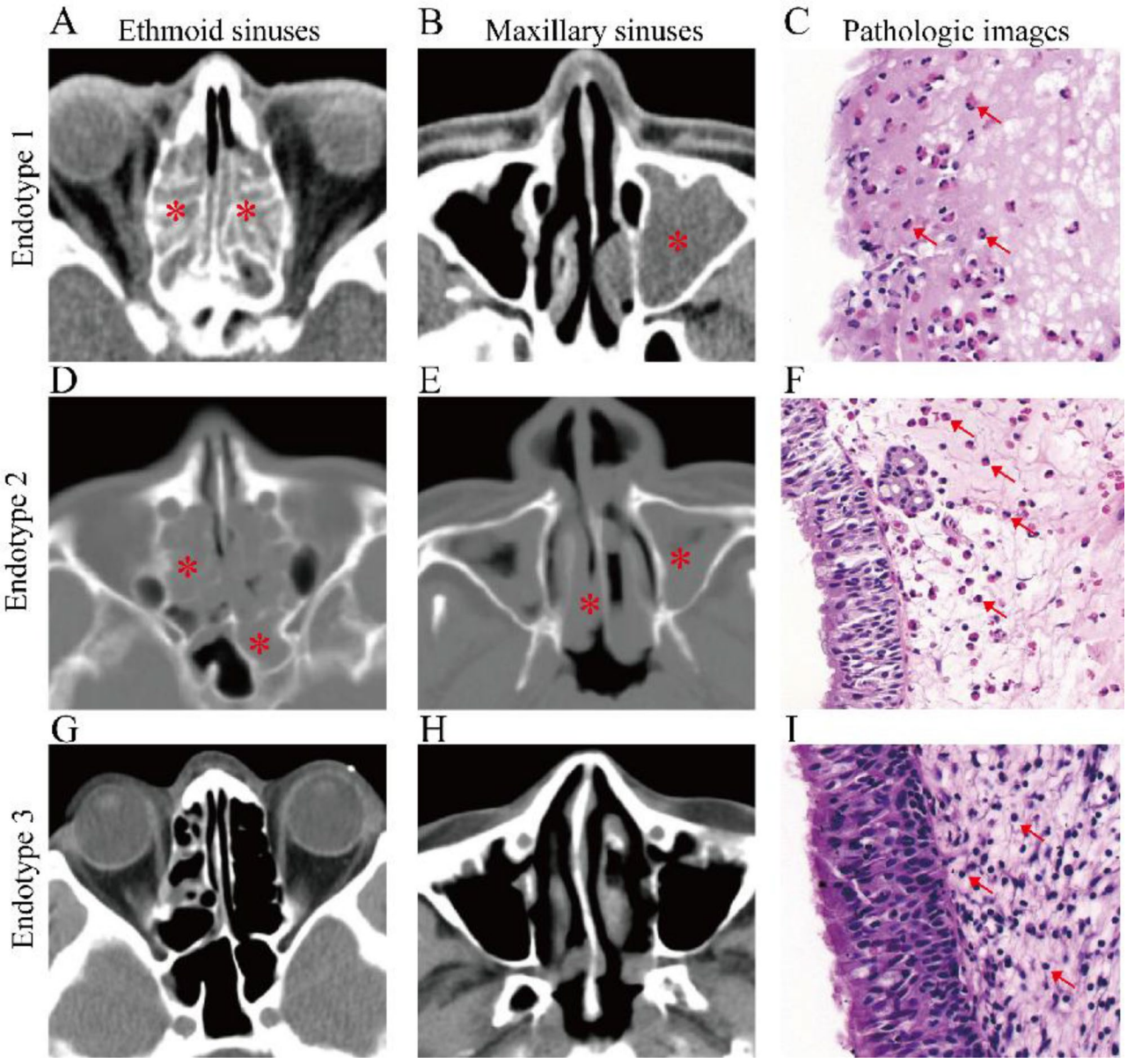

Fig. 4 Case examples demonstrating prognostic superiority of radiomic clustering. (**A**, **B**, **D**, **E**) CT of endotype 1 and 2: Diffuse pan-sinus opacification (asterisk) and polypoid middle meatal obstruction. (**C**, **F**) Histopathology of endotype 1 and 2: Hematoxylin-eosin (**H** & **E**) staining demonstrating eosinophil infiltration (arrowheads; scale bar: 100 μm). (**G**, **H**) CT of endotype 3: Bilateral mild ethmoid mucosal thickening with intact septa; patent ostiomeatal complex. (**I**) Histopathology of endotype 3: H&E staining revealing lymphocyte infiltration (arrowheads)

lipoproteins as potential protective factors in CRSwNP pathogenesis, exhibiting anti-inflammatory properties in mucosal epithelia [33–37]. Additionally, the β -alanine metabolic pathway enriched in this endotype was linked to anti-inflammatory and antioxidant effects [38, 39]. In general, endotype 2's superior prognosis may stem from enhanced fibrinolytic activity and lipoprotein-mediated anti-inflammatory pathways, suggesting novel therapeutic targets for recalcitrant CRSwNP. Clinically, endotype 3 was associated with higher Lund-Mackay/Kennedy scores [40]. Tissue-non-specific alkaline phosphatase (TNSALP) and zinc transporter 5 (ZnT5, an ALP activator [41]), were linked to enhanced bone formation [42–44] and zinc-mediated immunomodulation [45], suggesting poor prognosis. Besides, endotype 3 exhibited the highest levels of IgG/IgA immunoglobulin complexes, with elevated anti-dsDNA IgG/IgA autoantibodies implicating self-reactive B-cell activation in the polyp microenvironment [46]. These autoantibodies may also drive pathological complement activation [47, 48]. GO analysis further validated enriched B-cell-related pathways and complement activation, indicating concurrent

dysregulation of innate and adaptive immunity—a potential driver of chronic inflammation in CRSwNP [49]. This distinct immunophenotype suggests endotype 3 may represent an autoimmune-associated inflammatory endotype. Endotype 1, characterized by intermediate prognosis, exhibited a hybrid proteomic profile with co-enrichment of both lipoprotein-associated pathways and inflammatory pathways. This may reflect a transitional disease state in which the protective effects of lipid metabolism partially counteract the pro-inflammatory drive, leading to an intermediate patient prognosis. While mechanistic insights await further study, this heterogeneity highlights the inadequacy of binary classifications and highlights the value of radiomic-proteomic integration for nuanced stratification.

Despite our study's strengths, several limitations warrant acknowledgment. First, the single-center and retrospective design of our cohort constitutes a primary limitation that may affect the generalizability of our radiomics-derived endotypes. Future multicenter, prospective studies are essential for external validation and broader clinical translation. Second, the proteomic analysis was exploratory and conducted on a relatively small subset of patients ($n = 41$), limited by tissue availability. Although representative, larger multi-omics cohorts are needed to confirm the specific molecular pathways we identified and to achieve spatial correlation between imaging phenotypes and molecular activities. Finally, our endotypes are defined primarily based on radiomics features. A more comprehensive definition integrating inflammatory markers, genetics, and treatment responses could further refine these subtypes and enhance their clinical relevance in future studies.

This study provided an innovative non-invasive solution for endotyping in CRSwNP through CT-based radiomics technology. Unsupervised clustering identified three radiomic endotypes showing prognostic differences, with preliminary links to clinical phenotypes and proteomic profiles. From a clinical translation perspective, CT-based radiomic endotyping could be seamlessly incorporated into the routine preoperative evaluation workflow for patients with CRSwNP, as CT imaging is already standard practice and therefore does not impose additional patient burden. This approach enables preoperative identification of high-risk patients classified as Endotype 3 who require closer postoperative surveillance, regardless of their conventional eosinophilic phenotype. It also facilitates personalized follow-up strategies, whereby low-risk Endotype 2 patients may avoid unnecessary interventions, while Endotype 1 and Endotype 3 patients could benefit from tailored anti-inflammatory regimens. The external validation in an independent cohort of 270 patients further corroborated the prognostic value of these endotypes. Nevertheless, multicenter validation with longitudinal data is still required to confirm generalizability and clinical utility. If substantiated, this approach may complement preoperative risk assessment and inform personalized strategies, though its direct therapeutic implications need further investigation.

Supplementary Information

The online version contains supplementary material available at https://doi.org/10.1186/s12880-026-02369-1.

Supplementary Material 1

Acknowledgements
The authors thank the National Natural Science Foundation of China (82271146 and 82271147) and the Major Scientific and Technological Innovation Project of Shandong Province (2022CXGC020506) for supporting this work. We also thank all patients who participated in this study.

Author contributions
Xicheng Song, Ning Mao, and Hongfei Zhao contributed to the design and conception of the study. Hongfei Zhao, Qi Wang, Yan Hao, Pengyi Yu, Jingjing Li, Jianwei Wang, Yujuan Yang and Yakui Mou collected and analyzed the data. Hongfei Zhao and Qi Wang drafted the paper. Xicheng Song, Ning Mao and Yu Zhang contributed to the interpretation of the data. All authors contributed to the main text and read and approved the final version of the manuscript.

Funding
The research was supported by the National Natural Science Foundation of China (82271146 and 82271147), the Major Scientific and Technological Innovation Project of Shandong Province (2022CXGC020506).

Data availability
The datasets generated and analysed during the current study are not publicly available due to patient privacy and institutional data governance policies, but are available from the corresponding author on reasonable request.

Declarations

Ethics approval and consent to participate
The study protocol was approved by the Human Ethics Committee of Yantai Yuhuangding Hospital, Qingdao University (approval number: 2025-098) and conducted according to the principles of the Declaration of Helsinki. The requirement for written informed consent was partially waived for the retrospective study. Written informed consent was obtained from each patient before nasal polyp tissue sample collection.

Consent for publication
Not applicable.

Competing interests
The authors declare no competing interests.

Author details
[1]Qingdao Medical College, Qingdao University, Qingdao, China
[2]Department of Otorhinolaryngology, Head and Neck Surgery, Yantai Yuhuangding Hospital, Qingdao University, Yantai 264000, China
[3]Department of Radiology, Yantai Yuhuangding Hospital, Qingdao University, Yantai, Shandong 264000, China
[4]Shandong Provincial Clinical Research Center for Otorhinolaryngologic Diseases, Yantai, Shandong, China
[5]Big Data and Artificial Intelligence Laboratory, Yantai Yuhuangding Hospital, Qingdao University, Yantai, Shandong 264000, China
[6]Shandong Provincial Key Medical and Health Laboratory of Intelligent Diagnosis and Treatment for Women's Diseases, Yantai Yuhuangding Hospital, Qingdao University, Yantai, Shandong 264000, China

[7]Faculty of Applied Sciences, Macao Polytechnic University, Macao SAR 999078, China
[8]Shandong University of Traditional Chinese Medicine, Jinan, Shandong, China
[9]Department of Otorhinolaryngology Head and Neck Surgery, Xuanwu Hospital Capital Medical University, Beijing 100730, China

Received: 12 September 2025 / Accepted: 17 April 2026
Published online: 29 April 2026

References

1. Stevens WW, Schleimer RP, Kern RC. Chronic Rhinosinusitis with Nasal Polyps. J Allergy Clin Immunol Pract. 2016;4(4):565–72.
2. Bachert C, et al. Burden of Disease in Chronic Rhinosinusitis with Nasal Polyps. J Asthma Allergy. 2021;14:127–34.
3. Wen W, et al. Increased neutrophilia in nasal polyps reduces the response to oral corticosteroid therapy. J Allergy Clin Immunol. 2012;129(6):1522–e85.
4. Payne SC, et al. Evidence for distinct histologic profile of nasal polyps with and without eosinophilia. Laryngoscope. 2011;121(10):2262–7.
5. Alsharif S, et al. Endoscopic Sinus Surgery for Type-2 CRS wNP: An Endotype-Based Retrospective Study. Laryngoscope. 2019;129(6):1286–92.
6. Ho J, et al. Group 2 innate lymphoid cells (ILC2s) are increased in chronic rhinosinusitis with nasal polyps or eosinophilia. Clin Exp Allergy. 2015;45(2):394–403.
7. Fruth K, Gosepath J. Aspirin Exacerbated Respiratory Disease Adv Otorhinolaryngol. 2016;79:21–8.
8. Ghai S, et al. Comparison of Multiparametric MRI-targeted and Systematic Biopsies for Detection of Cribriform and Intraductal Carcinoma Prostate Cancer. Radiology. 2024;312(1):e231948.
9. Wu W, et al. Prediction of progression of interstitial lung disease in patients with systemic sclerosis: the SPAR model. Ann Rheum Dis. 2018;77(9):1326–32.
10. Spruit MA, et al. An official American Thoracic Society/European Respiratory Society statement: key concepts and advances in pulmonary rehabilitation. Am J Respir Crit Care Med. 2013;188(8):e13–64.
11. Lynch DA, et al. Diagnostic criteria for idiopathic pulmonary fibrosis: a Fleischner Society White Paper. Lancet Respir Med. 2018;6(2):138–53.
12. Arthur A, et al. A CT-based radiomics classification model for the prediction of histological type and tumour grade in retroperitoneal sarcoma (RADSARC-R): a retrospective multicohort analysis. Lancet Oncol. 2023;24(11):1277–86.
13. Wu G, et al. Structural and functional radiomics for lung cancer. Eur J Nucl Med Mol Imaging. 2021;48(12):3961–74.
14. Vagts C, et al. Unsupervised Clustering Reveals Sarcoidosis Phenotypes Marked by a Reduction in Lymphocytes Relate to Increased Inflammatory Activity on 18FDG-PET/CT. Front Med (Lausanne). 2021;8:595077.
15. Aerts HJ, et al. Decoding tumour phenotype by noninvasive imaging using a quantitative radiomics approach. Nat Commun. 2014;5:4006.
16. Migliozzi S, et al. Integrative multi-omics networks identify PKCdelta and DNA-PK as master kinases of glioblastoma subtypes and guide targeted cancer therapy. Nat Cancer. 2023;4(2):181–202.
17. Fokkens WJ, et al. European Position Paper on Rhinosinusitis and Nasal Polyps 2020. Rhinology. 2020;58(Suppl S29):1–464.
18. Lund VJ, Kennedy DW. Staging for rhinosinusitis. Otolaryngol Head Neck Surg. 1997;117(3 Pt 2):S35–40.
19. Lund VJ, Mackay IS. Staging in rhinosinusitus. Rhinology. 1993;31(4):183–4.
20. Foltyn-Dumitru M, et al. Cluster-based prognostication in glioblastoma: Unveiling heterogeneity based on diffusion and perfusion similarities. Neuro Oncol. 2024;26(6):1099–108.
21. Erich Schubert PJR. Faster k-Medoids clustering: improving the PAM, CLARA, and CLARANS algorithms. 2019 Oct 29. Available from: https://doi.org/10.48550/arXiv.1810.05691.
22. Tomassen P, et al. Inflammatory endotypes of chronic rhinosinusitis based on cluster analysis of biomarkers. J Allergy Clin Immunol. 2016;137(5):1449–e14564.
23. Brescia G, Alessandrini L, Marioni G. Structured histopathology for endotyping and planning rational treatment in chronic rhinosinusitis. Am J Otolaryngol. 2021;42(1):102795.
24. Mortuaire G, et al. Histopathological classification of refractory chronic rhinosinusitis with nasal polyps. Histol Histopathol. 2015;30(12):1447–54.
25. Hao D, et al. An Integrated Analysis of Inflammatory Endotypes and Clinical Characteristics in Chronic Rhinosinusitis with Nasal Polyps. J Inflamm Res. 2022;15:5557–65.
26. Wang X, et al. Endotypes of chronic rhinosinusitis based on inflammatory and remodeling factors. J Allergy Clin Immunol. 2023;151(2):458–68.
27. Xu Z, et al. CGUFS: A clustering-guided unsupervised feature selection algorithm for gene expression data. J King Saud Univ Comput Inf Sci. 2023;35(9):101731.
28. Zhu KZ, et al. Development and multicenter validation of a novel radiomics-based model for identifying eosinophilic chronic rhinosinusitis with nasal polyps. Rhinology. 2023;61(2):132–43.
29. Hua HL, et al. Differentiation of eosinophilic and non-eosinophilic chronic rhinosinusitis on preoperative computed tomography using deep learning. Clin Otolaryngol. 2023;48(2):330–8.
30. Bachert C, et al. Nasal polyposis: from cytokines to growth. Am J Rhinol. 2000;14(5):279–90.
31. Takabayashi T, et al. Excessive fibrin deposition in nasal polyps caused by fibrinolytic impairment through reduction of tissue plasminogen activator expression. Am J Respir Crit Care Med. 2013;187(1):49–57.
32. Del Rosso M, et al. The plasminogen activation system in inflammation. Front Biosci. 2008;13:4667–86.
33. Chung YW, et al. Apolipoprotein E and Periostin Are Potential Biomarkers of Nasal Mucosal Inflammation. A Parallel Approach of In Vitro and In Vivo Secretomes. Am J Respir Cell Mol Biol. 2020;62(1):23–34.
34. Tomazic PV, et al. Apolipoproteins have a potential role in nasal mucus of allergic rhinitis patients: a proteomic study. Laryngoscope. 2015;125(3):E91–6.
35. Singh K, et al. The apolipoprotein E-mimetic peptide COG112 inhibits the inflammatory response to Citrobacter rodentium in colonic epithelial cells by preventing NF-kappaB activation. J Biol Chem. 2008;283(24):16752–61.
36. Yao X, Remaley AT, Levine SJ. New kids on the block: the emerging role of apolipoproteins in the pathogenesis and treatment of asthma. Chest. 2011;140(4):1048–54.
37. El-Bahrawy AH, et al. Correction: ApoE deficiency promotes colon inflammation and enhances the inflammatory potential of oxidized-LDL and TNF-alpha in primary colon epithelial cells. Biosci Rep. 2016;36(6).
38. Meftahi GH, Jahromi GP. Biochemical Mechanisms of Beneficial Effects of Beta-Alanine Supplements on Cognition. Biochem (Mosc). 2023;88(8):1181–90.
39. Luo W, et al. Reposition: focalizing beta-alanine metabolism and the anti-inflammatory effects of its metabolite based on multi-omics datasets. Int J Mol Sci. 2024;25(19).
40. Brooks SG, et al. Preoperative Lund-Mackay computed tomography score is associated with preoperative symptom severity and predicts quality-of-life outcome trajectories after sinus surgery. Int Forum Allergy Rhinol. 2018;8(6):668–75.
41. Suzuki T, et al. Zinc transporters, ZnT5 and ZnT7, are required for the activation of alkaline phosphatases, zinc-requiring enzymes that are glycosylphosphatidylinositol-anchored to the cytoplasmic membrane. J Biol Chem. 2005;280(1):637–43.
42. Snidvongs K, Sacks R, Harvey RJ. Osteitis in Chronic Rhinosinusitis. Curr Allergy Asthma Rep. 2019;19(5):24.
43. Georgalas C, et al. Global Osteitis Scoring Scale and chronic rhinosinusitis: a marker of revision surgery. Clin Otolaryngol. 2010;35(6):455–61.
44. Huang Z, et al. Clinical predictors of neo-osteogenesis in patients with chronic rhinosinusitis. Int Forum Allergy Rhinol. 2015;5(4):303–9.
45. Kim B, Lee WW. Regulatory Role of Zinc in Immune Cell Signaling. Mol Cells. 2021;44(5):335–41.
46. Tan BK, et al. Evidence for intranasal antinuclear autoantibodies in patients with chronic rhinosinusitis with nasal polyps. J Allergy Clin Immunol. 2011;128(6):1198–e12061.
47. Huang J, Xu Y. Autoimmunity: a new focus on nasal polyps. Int J Mol Sci. 2023;24(9).
48. Van Roey GA, et al. Classical complement pathway activation in the nasal tissue of patients with chronic rhinosinusitis. J Allergy Clin Immunol. 2017;140(1):89–e1002.
49. Schleimer RP. Immunopathogenesis of Chronic Rhinosinusitis and Nasal Polyposis. Annu Rev Pathol. 2017;12:331–57.

Publisher's note